Directed integration of ZnO nanobridge sensors using photolithographically patterned carbonized photoresist

2010 Nanotechnology 21 195307

(http://iopscience.iop.org/0957-4484/21/19/195307)

Nanotechnology **21** (2010) 195307 (7pp) doi:10.1088/0957-4484/21/19/195307

Directed integration of ZnO nanobridge sensors using photolithographically patterned carbonized photoresist

Chien-Chih Huang, Brian D Pelatt and John F Conley Jr

School of Electrical Engineering and Computer Science, Oregon State University, Corvallis, OR, USA

E-mail: huangch@onid.orst.edu

Received 9 February 2010, in final form 31 March 2010
Published 21 April 2010
Online at stacks.iop.org/Nano/21/195307

Abstract

A method for achieving large area integration of nanowires into electrically accessible device structures remains a major challenge. We have achieved directed growth and integration of ZnO nanobridge devices using photolithographically patterned carbonized photoresist and vapor transport. This carbonized photoresist method avoids the use of metal catalysts, seed layers, and pick and place processes. Growth and electrical connection take place simultaneously for many devices. Electrical measurements on carbonized photoresist/ZnO nanobridge/carbonized photoresist structures configured as three-terminal field effect devices indicate bottom gate modulation of the conductivity of the n-type ZnO channel. Nanobridge devices were found to perform well as ultraviolet and gas sensors, and were characterized as regards ultraviolet light pulsing, oxygen concentration, and humidity. The sensitivity of the three-terminal nanobridge sensors to UV light and oxygen was enhanced by application of a negative bottom gate voltage.

1. Introduction

Due in part to an inherently large surface to volume ratio, metal oxide nanowires (NWs), such as ZnO, offer great promise for gas and UV sensing applications [1–10]. However, because NWs are quasi-one-dimensional structures, integrating them into electrically accessible device structures remains a challenge. Much of the NW device and sensor work to date has been demonstrated using individual devices constructed using the 'pick and place' method and NWs grown via the vapor–liquid–solid (VLS) method [11]. In the 'pick and place' method, NWs are collected from a growth substrate by applying an external force (such as sonication), dispersed into solution, and then transferred randomly onto a device substrate. Device fabrication proceeds either via a low yield top down flow or via sophisticated processes such as scanning electron microscopy (SEM), electron beam lithography [4, 7], and/or focus ion beam deposition [12], which are used to find and make electrical contact to individual NW devices. Due to drawbacks such as a broad NW size distribution following sonication, random placement, potential contamination during NW transfer between different substrates, and low throughput/yield, the 'pick and place' method is not suitable for wafer scale manufacturing.

Wafer scale integration into a manufacturable process requires alignment of the NWs to lithographically defined features. An integration approach that addresses this requirement is the directed growth of NW nanobridge devices in which a NW is grown from one electrode to terminate on an opposing electrode [3, 6, 13–17]. A major advantage of the nanobridge method is that NWs are selectively grown and used in place—no further steps are required to 'harvest', align, or to make electrical contact to the NWs. Formation of Si nanobridges across a trench on a silicon-on-insulator (SOI) substrate by using a patterned Au catalyst to direct growth was first reported by Islam *et al* [13, 15]. Some drawbacks to this approach are the difficulty of patterning Au, contamination from residual Au, and the use of an expensive SOI substrate. The direct formation of ZnO nanobridge devices has been reported using a patterned ZnO seed layer [3, 14, 16, 17] to direct growth. Despite the avoidance of a metal catalyst, the seed layer method still has drawbacks such as the use of an SOI substrate, reactive ion etching for trench formation, and deposition and patterning of the seed layer.

Recently, a novel method for selective NW growth was reported in which carbonized photoresist (C-PR) is used as a nucleation layer for the selective and oriented growth of ZnO nanowires from evaporated ZnO powder [18–20]. Although nanobridge structures were not fabricated and electrical measurements of NWs were not performed, the relatively small lateral shrinkage of PR during the carbonization process [21–23] and the low resistivity of C-PR films (comparable to indium–tin-oxide (ITO) [18]), suggests that patterned C-PR pads could be used to make direct electrical contact to integrated NW devices.

In this work, we use C-PR to simultaneously grow and electrically integrate ZnO nanobridge three-terminal bottom gate field effect devices. The use of C-PR offers several potential advantages for the formation of nanobridge devices including avoiding deposition/patterning of a seed or catalyst layer, avoiding potential metal contamination, easy patterning of PR prior to carbonization, and the use of C-PR as both a nucleation layer for selective NW growth and an electrode for electrical contact. We characterize the UV, oxygen, and H_2O sensing properties of ZnO nanobridge sensors and demonstrate that NW devices and sensors based on C-PR nanobridges perform comparably to NW devices that have been synthesized based on the 'pick and place' method [24]. Furthermore, we show that the UV and oxygen sensing properties can be enhanced by operating the nanobridge sensors as three-terminal devices with a negative voltage applied to the bottom gate [5, 8].

2. Materials, methods, and device fabrication

2.1. Materials and methods

Carbonized Microchem S1818 photoresist (PR) was used to direct the growth and formation of ZnO nanobridges. Carbonization was accomplished by baking the S1818 PR for 60 min at 900 °C and 5 Torr in a reducing atmosphere (95% Ar, 5% H_2) (described more fully in [23]). Molybdenum (Mo) was deposited via evaporation and patterned using a liftoff process. Nanobridges were grown between adjacent C-PR pads via carbothermal reduction of ZnO using pure ZnO (99.99%, Sigma-Aldrich) and graphite powders (99.9995%, Alpha Aeser) mixed in a 1:1 ratio [31]. The mixture was placed in a tube furnace at 920 °C and a flow of 150 sccm N_2 was used to carry it downstream to the substrates, placed at 770 °C. 1–2 sccm of O_2 was introduced 2.5 cm from the samples to aid in nanobridge growth.

The C-PR thickness was measured with an Alpha Step Surface Profiler. NW length, diameter, and orientation were characterized using an FEI dual beam field emission scanning electron microscope (FESEM). Electrical measurements were performed using an Agilent 4155C Semiconductor Parameter Analyzer. The UV response was measured using a Mineralight 254 nm, 18.4 W lamp as an excitation source. The gas sensing response was measured using an Agilent B1500 Semiconductor Parameter Analyzer, a NorECs ProboStat high temperature measurement cell, a tube furnace for temperature control, and 200 sccm mass flow controllers (MFCs) to control gas flow rates.

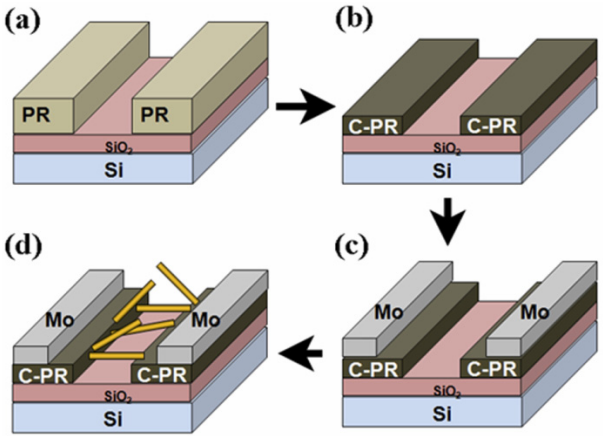

Figure 1. Schematic process flow for nanobridge growth on C-PR. (This figure is in colour only in the electronic version)

2.2. Nanobridge device fabrication using carbonized photoresist

Construction of nanobridges using C-PR was composed of four main steps, as schematically illustrated in figure 1. First, PR was coated on thermally grown SiO_2 coated Si wafers and patterned using conventional contact lithography (figure 1(a)). Next, the PR was carbonized at 900 °C in a reducing atmosphere (figure 1(b)). During the carbonization process, the PR was found to shrink by ∼80% vertically, but only 1–2% laterally, roughly consistent with previously reported C-PR results [22, 23]. Third, Mo was patterned over part of the C-PR, as shown in figure 1(c). Finally, NWs were synthesized on the patterned C-PR substrates to form ZnO nanobridge devices between adjacent pads, shown in figure 1(d).

Although C-PR pads were measured to have an initial resistivity of 4.22×10^{-3} Ω cm, consistent with a previous report [22], we found that the NW growth process increased pad resistivity by about a factor of five, to 2.34×10^{-2} Ω cm. The resistivity increase may be related to the formation of a ZnO NW layer on the surface of the C-PR or further vertical shrinkage of CP-R due to the existence of a small amount of residual oxygen during NW growth. To reduce overall contact resistance to the ZnO nanobridges, a thin film of Mo was used to coat the C-PR away from the nanobridge region. Mo was chosen because it does not support the growth of ZnO NWs (see figure 2), has good thermal stability, and low thermal expansion. Besides reducing electrical resistance between contact probes and the nanobridges, the high density of the Mo reduces electrode damage due to probe contact and may also protect the C-PR from oxidization during high temperature NW growth processing.

Scanning electron microscopy (SEM) images of completed nanobridge device structures are shown in figure 2. The selective growth of ZnO NWs on the C-PR region can be observed in the low magnification image in 2(a) as well as the higher magnification image in figure 2(b). NW growth occurs primarily on the C-PR region and at the edges of the Mo region where the C-PR is exposed. ZnO NWs were not observed on

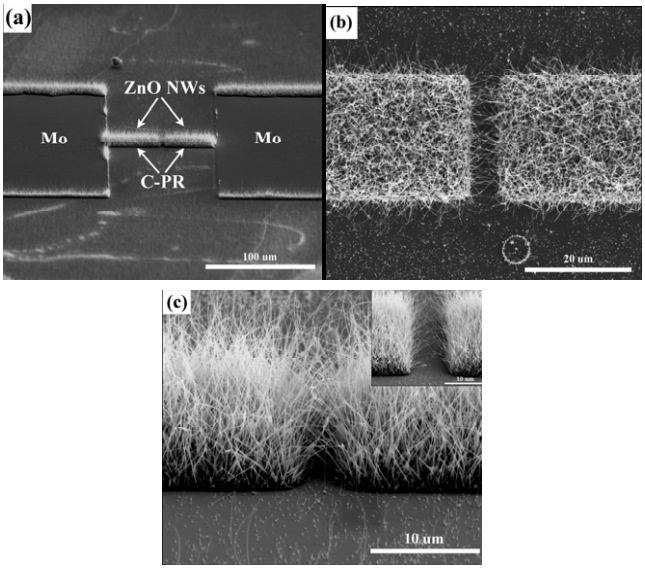

Figure 2. SEM images of (a) the complete structure with Mo pad, (b) zoomed in top view and (c) zoomed in side view of ZnO nanobridges across a 5 μm trench. Inset in (c) shows nanobridges across a 10 μm trench.

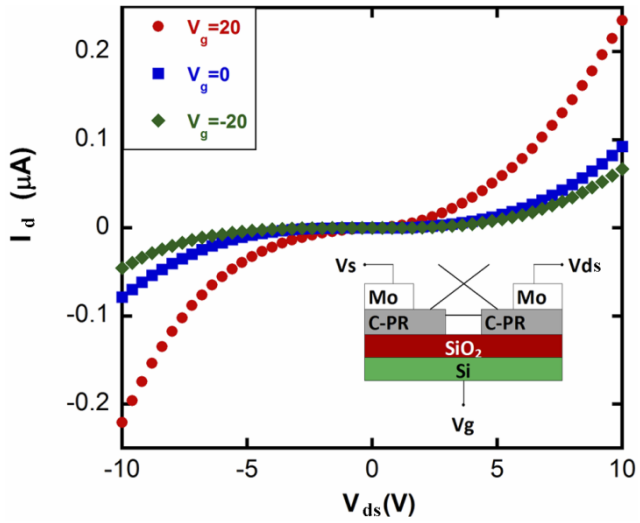

Figure 3. I_d–V_{ds} plot for a 5 μm gap nanobridge device at various values of back gate bias, V_g.

the Mo coated region and only sparsely distributed short ZnO NWs (<3 μm) could be found on the SiO_2 surface.

ZnO NWs 5–15 μm in length and 60–120 nm in diameter were grown roughly normal to the surface of the 300 nm C-PR film. The top down SEM image in figure 2(b) reveals that a number of nanobridges were formed across the 5 μm gap between C-PR pads. The angled side view SEM image of the 5 μm gap device in figure 2(c) reveals that NW connections between the opposing C-PR pads can be made in several ways: (i) direct connection by a single wire, (ii) fusing of two wires from two pads, and (iii) possible connection by physical touching of two wires. Owing to the thin layer (300 nm) of C-PR, the majority of the NW connections are of types (ii) and (iii) and thus form a three-dimensional nanobridge network structure. The SEM image of a 10 μm gap in the inset shows that a lower density of bridges are formed across the increased gap. An advantage of this type of structure over a typical two-dimensional structure is the potential for higher sensitivity for sensing applications due to increased NW surface area available per unit substrate area.

3. Results and discussion

3.1. Current–voltage characteristics

We find that the nanobridges form conductive paths between the C-PR electrodes and can be operated as three-terminal field effect devices by using the silicon back contact as the gate electrode with SiO_2 and air acting as the gate dielectric. Shown in figure 3 is a plot of pad to pad current (I_d) versus pad to pad voltage (V_{ds}) for three different back gate bias (V_g) conditions for a 10 μm C-PR pad separation ZnO nanobridge device. The curvature of the I_d–V_{ds} traces indicates the Schottky nature of the C-PR contact to the nanobridges [25]. Although a Schottky-type contact is not ideal for FET operation, Zhou *et al*, have reported that the Schottky barrier can be helpful for UV sensing by reducing electron–hole recombination rate and increasing carrier density [7]. If was found that V_g can be used to modulate I_d. As shown in figure 3, because ZnO is intrinsically an n-type semiconductor, application of positive V_g enhanced conductance and increased I_d due to an accumulation of carriers. On the other hand, a negative V_g resulted in a decrease in I_d due to a depletion of charge carriers [26].

3.2. Ultraviolet sensing

ZnO NWs are well known to be sensitive to ultraviolet (UV) light [3, 6–10]. Figure 4 shows the response of a 5 μm gap nanobridge device to 30 s pulses of UV light (254 nm; 3 mW cm^{-2}) in air with $V_{ds} = 3$ V and a floating V_g. During repeated UV exposures, I_d increases roughly 500× upon UV exposure, stays roughly constant during UV exposure, and then returns to the pre-exposure value after the UV exposure ends. The rise time (the time it takes for the current to reach 90% of its maximum value) [27] is roughly 1.2 s, and the decay time (the time it takes for the current to decrease to 10% of its maximum value) is roughly 3.4 s. Table 1 shows that these rise and decay times are comparable to other reported results, suggesting a fast and effective response to UV illumination.

Besides photogenerated carriers, the ZnO nanobridge photoresponse is also strongly influenced by desorption and reabsorption of O_2 and H_2O molecules on the nanobridge surface. The reason for the decay times being typically longer than the rise times (table 1), particularly after the initial 90% recovery as seen in figures 4 and 5, is likely due to slow reabsorption and interaction of O_2 and H_2O molecules with the nanobridge surface [28]. Upon UV illumination, electron–hole pairs are immediately created inside the ZnO nanobridges resulting in increased conductivity. As described by Li *et al* [28], the newly created holes drift towards

Table 1. ZnO nanowire UV response comparison for different research groups.

Group	Rise time (s)	Decay time (s)	Light source	I_{UV}/I_{dark}
This work	1.2	4.4	254 nm; ∼3 mW cm^{-2}	400–1000[a]
Kim [8]	—	47	365 nm; 0.47 mW cm^{-2}	10^{6}[a]
Li [6]	0.7	1.4	350 nm; 10^{-8}–10^{-2} W cm^{-2}	10–10^{5}
Zhou [7]	0.6	6	365 nm; 30 μW cm^{-2}	1500
Jeong [9]	4	30	350 nm; 1 mW cm^{-2}	10
Law [10]	0.4 × 10^{-3}	0.36 × 10^{-3}	370 nm	1.15
Conley [3]	1	180	—	10^{2}

[a] I_{UV}/I_{dark} are optimized by applying gate voltage.

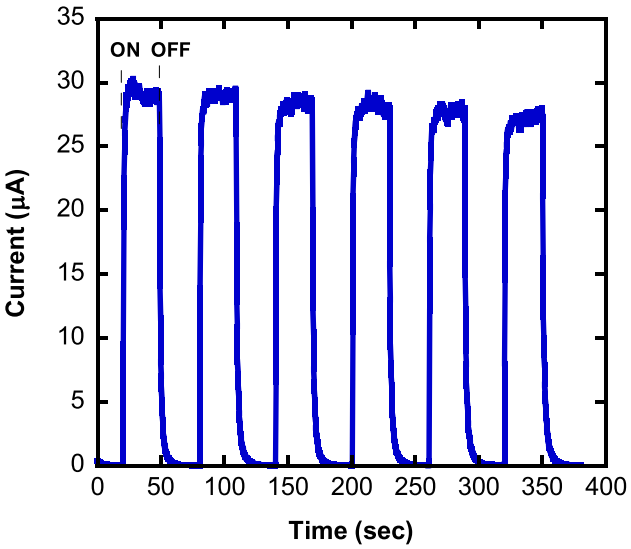

Figure 4. Photoresponse as a function of time for a 5 μm nanobridge device with $V_{ds} = 3$ V exposed to 30 s pulses of UV light.

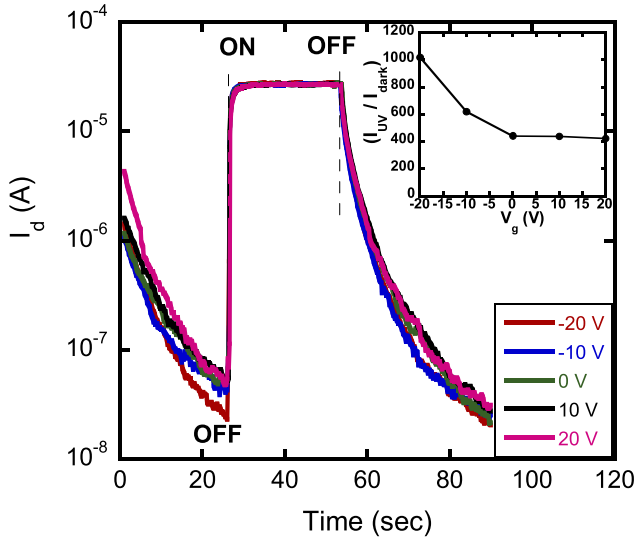

Figure 5. UV photoresponse as a function of time for nanobridge devices under various gate voltages, V_g. Inset shows normalized drain current (I_{UV}/I_{dark}) as a function of V_g with $V_{ds} = 3$ V.

the surface (under the influence of upward band bending) where they discharge chemisorbed negatively charged O_2 ions (O_2^-(ad) + $h^+ \rightarrow O_2$(g)), leaving behind excess unpaired electrons which further increase the conductivity. When the UV light is switched off, the excess holes and electrons recombine, immediately reducing conductivity. Meanwhile, O_2 gradually reabsorbs onto the surface, taking up additional electrons, creating a depletion region, and further reducing the conductivity. Thus, the decay time of UV induced photocurrent will be strongly influenced by the presence of O_2 in the ambient. It is likely that the long decay time seen, for example, in Conley *et al* [3] was due to the UV response being measured with dry N_2 flowing over the device.

The interaction of H_2O molecules with the ZnO NW surface is more complex [28]. In the dark, H_2O molecules can increase NW conductivity by displacing adsorbed O_2 molecules. Unlike O_2 molecules, which capture only electrons, dissociated H_2O molecules can simultaneously attract both electrons and holes. For prolonged UV exposure in a high humidity ambient, this can decrease the overall carrier density and thus the photocurrent. Since the number of excess unpaired electrons is reduced during illumination by the presence of H_2O molecules displacing O_2 molecules on the surface, less excess electrons remain after electron–hole recombination, which results in faster current decay upon switching off the UV light.

The existence of H_2O molecules in the measurement ambient might also be used to explain the slight monotonic decrease in the magnitude of the photoresponse during subsequent UV pulses (figure 4). Since O_2 will be desorbed from the surface during UV illumination, the NW surface may attract H_2O molecules. Although in the dark, adsorbed H_2O molecules are replaced gradually by O_2 due to the lower thermal stability of H_2O molecules relative to O_2 molecules on the ZnO surface [29], the 30 s period between subsequent pulses may not be enough time for H_2O and O_2 on the surface of the NW to return to the equilibrium state. Therefore the H_2O concentration on the surface of the ZnO NWs may gradually increase during pulsed UV exposure, which could lead to the observed slight decrease in photocurrent. According to [28], the relatively flat response of I_d during an individual UV pulse (figures 4 and 5) suggests that the relative humidity during our UV response measurements was less than roughly 70%.

The back gate bias was found to have an influence on UV photoresponse. Shown in figure 5 are plots of I_d versus time for a 5 μm gap nanobridge device exposed to a 30 s UV pulse with $V_{ds} = 3$ V and for various back gate voltages, V_g. In an

attempt to provide a common starting point, the data in figure 5 was captured beginning 5 s after the end of a previous 30 s UV pulse. When UV is initially switched on (at $t \sim 25$ s), the photocurrent (I_{UV}) increases rapidly (within 1.2 s) to around 30 μA, regardless of applied V_g. Once the UV is switched off (at $t \sim 55$ s), it is found that the decay time of I_d (the time it takes for I_d to decrease to 10% of its maximum value) increases slightly with increasing negative V_g, ranging from 3.8 s for $V_g = -20$ V to 4.8 s for $V_g = 20$ V. The V_g dependence is similar to that reported by Kim *et al* [8] for single NW devices. Shown in the inset of figure 5 is a plot of the normalized UV response magnitude versus V_g. The magnitude of the UV response is normalized by dividing I_{UV} (I_d measured after UV was turned on for 5 s) by the value of I_d in the dark (I_{dark}, taken as the value of I_d immediately preceding the light pulse). The I_{UV}/I_{dark} ratio ranges from as high as 10^3 when a negative back gate voltage $V_g = -20$ V is applied to approximately 400 for $V_g \geqq 0$ V. As I_{UV} is almost the same for all V_g (under UV illumination, the nanobridges have effectively degenerate carrier density), the increase of I_{UV}/I_{dark} ratio for negative V_g is due to the dependence of I_{dark} on V_g. The observed V_g dependence of UV sensitivity can be related to the change of carrier concentration. According to Kim *et al* [8] the UV sensitivity of a ZnO NW FET can be optimized when V_g is set below the threshold voltage, so as to deplete the NW of carriers and reduce I_{dark} [10]. As shown in figure 3, our n-type ZnO NWs can be depleted at negative V_g. The carrier concentration in the nanobridges can be roughly estimated using [30]:

$$n_e = \frac{V_{on} C_g}{q \pi r^2 L} \tag{1}$$

and

$$C_g = \frac{2\pi\varepsilon\varepsilon_0 L}{\ln \frac{2h}{r}} \tag{2}$$

where q is the charge of the electron, r is the cumulative radius of the NWs, L is the length of the NW channel, and ε and h are the effective dielectric constant and effective thickness of the gate dielectric (SiO_2 and air).

Because our devices are composed of a collection of nanobridges at various heights above the substrate (see figure 2(c)), the wide range of effective dielectric thickness, h, results in a variation in the response of carrier concentration to applied V_g, or stretch-out of the I_d–V_{ds} characteristic. Under a fixed negative V_g, once the UV switches off, the NWs close to the substrate will turn off first. With increasing negative V_g, additional NWs further from the substrate will also become depleted and result in a further decrease of I_{dark}. Therefore, unlike single NW FET devices which showed strong V_g dependent UV response that abruptly saturates at negative voltages [8], the 3D nature of our nanobridge devices results in a weaker and broader V_g response. For similar reasons, the V_g dependence of the post-UV I_d decay time that can be seen in figure 5 (decay time increasing with increased positive V_g) is also qualitatively similar but quantitatively weaker than that reported for single NW devices [8].

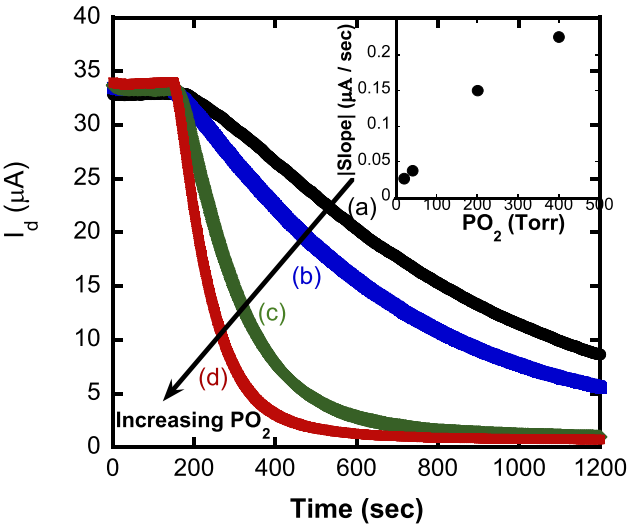

Figure 6. Plot of I_d versus time for a 5 μm nanobridge device with $V_{ds} = 3$ V as a function of oxygen partial pressure (P_{O_2}). Shown are (a) 20 Torr, (b) 40 Torr, (c) 200 Torr and (d) 400 Torr. Inset shows absolute value of the initial slope at time = 205 s.

3.3. Oxygen sensing

We also demonstrate operation of C-PR/ZnO nanobridge devices as gas sensors. Shown in figure 6 is a plot of I_d versus time as a function of O_2 partial pressure (P_{O_2}) for a 5 μm gap nanobridge device measured at 150 °C with $V_{ds} = 3$ V. P_{O_2} was controlled by varying the ratio of N_2 and O_2 flow rates at a fixed total flow rate of 200 sccm. It is well known that operation of metal oxide based gas sensors at elevated temperature allows for more rapid saturation and faster sensor response [32]. Prior to each measurement, the sample was annealed for 5 h at 150 °C under 200 sccm flow of pure N_2 gas to accelerate desorption of O_2 and achieve saturation of I_d as an initial starting current. To take advantage of the stable initial current, measurement were performed at the same temperature, 150 °C. I_d decreases as O_2 is introduced. As discussed in section 3.2, O_2 gradually chemisorbs onto the NW surface, capturing electrons to become negatively charged and reducing the conductivity. The time it takes for the O_2 to saturate the NW surface is a function of P_{O_2}. At high P_{O_2}, O_2 quickly saturates the surface of the NWs and I_d quickly saturates at a lower value. At low P_{O_2}, I_d does not show saturation even after 20 min of continuous O_2 flow. Shown in the inset is a plot of initial slope of the O_2 induced current decay versus P_{O_2}. The initial slope is extracted at a time of 205 s. From the inset it is seen that higher P_{O_2} leads to a steeper initial decay rate resulting in faster I_d saturation.

O_2 sensitivity was also found to be a function of V_g. Figure 7 shows nanobridge response to O_2 ($P_{O_2} = 40$ Torr) as a function of time for various V_g. The magnitude of the O_2 response is normalized by dividing the current during O_2 exposure ($I_{O_2}(t)$) by the stabilized current in a N_2 ambient (I_{N_2}). As was seen for the magnitude of UV response, the magnitude of the O_2 response increases as V_g decreases toward negative voltages. The gate dependence of the O_2 response can be explained by the ratio of total electrons to electrons

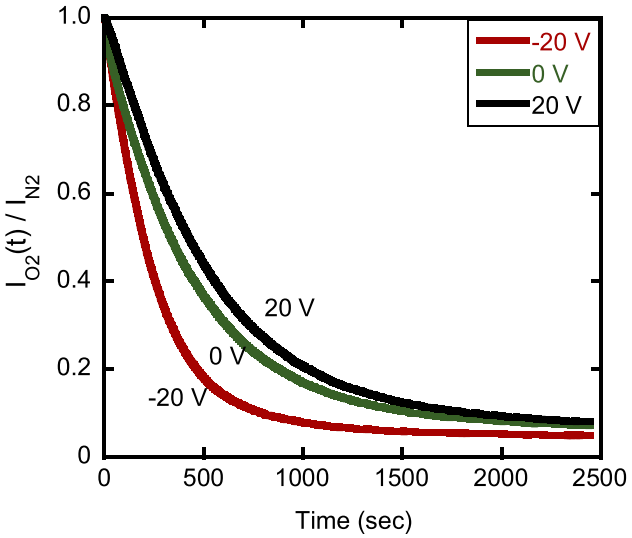

Figure 7. Plot of normalized current response during O_2 exposure ($I_{O_2}(t)/I_{N_2}$) versus time as a function of gate voltage (V_g) for a 5 μm device with $P_{O_2} = 40$ Torr and $V_{ds} = 3$ V at a measurement temperature of 150 °C.

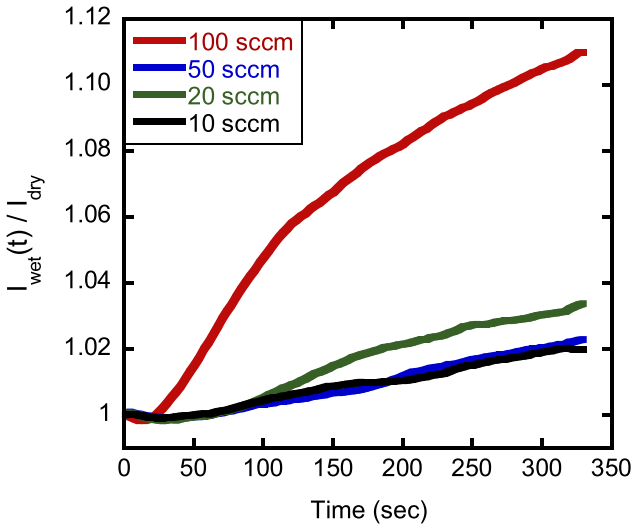

Figure 8. Plot of normalized current ($I_{wet}(t)/I_{N_2}$) versus time for a 5 μm devices exposed to wet N_2 flow rates of 100, 50, 20, and 10 sccm. The V_{ds} is 3 V and the measurement temperature is 150 °C.

captured by surface O_2 [5]. Since ZnO nanobridges are n-type, a positive gate voltage increases electron concentration within the nanobridge channel. In this case, the electrons captured by adsorbed O_2 molecules represent a reduced portion of the total electrons in the nanobridge, leading to a reduced O_2 response compared to $V_g = 0$ V. When V_g is negative, the electron concentration in the nanobridge is diminished and the electrons captured by surface O_2 will represent a greater relative proportion of the total electrons, leading to enhanced O_2 response.

3.4. Humidity sensing

A preliminary characterization of the response of the nanobridge devices to humidity was also performed. Similar to our control of O_2 concentration, the humidity level was roughly adjusted by changing the ratio of flow rates for 'wet' N_2 and dry N_2 at a fixed total flow rate (200 sccm). The wet N_2 was generated by flowing dry N_2 through a bubbler filled with DI water at room temperature. Various concentrations of wet N_2/dry N_2 mixtures were flown over devices at 150 °C for 5 min. In between wet N_2 exposures, devices were flushed with dry N_2 for 10 min. Shown in figure 8 is a plot of normalized I_d ($I_{wet}(t)/I_{dry}$) for a 5 μm gap device with $V_{ds} = 3$ V and a floating V_g for various flow rates of wet N_2 at 150 °C. I_d increases as a function of time during wet N_2 exposure and recovers between exposures. As discussed in section 3.2, H_2O molecules can interact with the ZnO NW surface to increase conductivity by either directly donating an electron or by displacing a chemi-adsorbed O_2 [28] to release a trapped electron. The magnitude of the response is greatest for the highest wet N_2 flow rate (100 sccm). Nanobridge response roughly decreases with decreasing wet N_2 flow rate. However, it is seen that the 50 sccm response is lower than the 20 sccm response. The 50 sccm response was the final one in the experimental sequence and it is possible that H_2O absorbed on the ZnO NW surface during several experiments at 150 °C contributed to the decreased sensitivity.

4. Conclusion

We demonstrate a simple method to fabricate ZnO nanobridge sensors and bottom gate FET structures using C-PR both for nanowire nucleation and electrical contact. The use of PR allows for easy patterning of the force that directs NW growth and avoids both (i) deposition and patterning of a metal catalyst with its potential for contamination and (ii) deposition and patterning of a seed layer. Electrical connection to the nanowires occurs simultaneously with nanowire growth. Despite Schottky-type contact between the C-PR and the ZnO nanowires, nanobridge devices were operated effectively as sensors and were characterized for UV, O_2, and H_2O sensitivity. The UV response of the nanobridge devices is comparable to results reported for devices fabricated using the pick and place method. We also found that the current across a three-terminal nanobridge device could be modulated by a bottom gate voltage. In addition, detection sensitivity to UV and O_2 was found to be enhanced by application of negative bottom gate voltages. Because nanobridge growth is selectively directed between photolithographically defined electrodes and nanobridges are used in place, the C-PR technique has the potential for wafer scale integration of nanodevices.

Acknowledgments

The authors are grateful to the Army Research Lab (W911NF-07-2-0083), the Office of Naval Research (N00014-07-1-0457), and ONAMI for support. The authors also thank Chris Tasker for assistance with experimental setup.

References

[1] Agarwal R and Lieber C M 2006 Semiconductor nanowires: optics and optoelectronics *Appl. Phys.* A **85** 209–15

[2] Kolmakov A and Moskovits M 2004 Chemical sensing and catalysis by one-dimensional metal-oxide nanostructures *Annu. Rev. Mater. Res.* **34** 151–80

[3] Conley J F, Stecker L and Ono Y 2005 Directed integration of ZnO nanobridge devices on a Si substrate *Appl. Phys. Lett.* **87** 223114

[4] Cui Y, Wei Q Q, Park H K and Lieber C M 2001 Nanowire nanosensors for highly sensitive and selective detection of biological and chemical species *Science* **293** 1289–92

[5] Fan Z Y, Wang D W, Chang P C, Tseng W Y and Lu J G 2004 ZnO nanowire field-effect transistor and oxygen sensing property *Appl. Phys. Lett.* **85** 5923–5

[6] Li Y B, Della Valle F, Simonnet M, Yamada I and Delaunay J J 2009 High-performance UV detector made of ultra-long ZnO bridging nanowires *Nanotechnology* **20** 045501

[7] Zhou J, Gu Y D, Hu Y F, Mai W J, Yeh P H, Bao G, Sood A K, Polla D L and Wang Z L 2009 Gigantic enhancement in response and reset time of ZnO UV nanosensor by utilizing Schottky contact and surface functionalization *Appl. Phys. Lett.* **94** 191103

[8] Kim W and Chu K S 2009 ZnO nanowire field-effect transistor as a UV photodetector optimization for maximum sensitivity *Phys. Status Solidi* a **206** 179–82

[9] Jeong M C, Oh B Y, Lee W and Myoung J M 2005 Optoelectronic properties of three-dimensional ZnO hybrid structure *Appl. Phys. Lett.* **86** 103105

[10] Law J B K and Thong J T L 2006 Simple fabrication of a ZnO nanowire photodetector with a fast photoresponse time *Appl. Phys. Lett.* **88** 133114

[11] Wagner R S, Ellis W C, Jackson K A and Arnold S M 1964 Study of the filamentary growth of silicon crystals from the vapor *J. Appl. Phys.* **35** 2993–3000

[12] He J H, Chang P H, Chen C Y and Tsai K T 2009 Electrical and optoelectronic characterization of a ZnO nanowire contacted by focused-ion-beam-deposited Pt *Nanotechnology* **20** 135701

[13] Islam M S, Sharma S, Kamins T I and Williams R S 2005 A novel interconnection technique for manufacturing nanowire devices *Appl. Phys.* A **80** 1133–40

[14] Conley J F, Stecker L and Ono Y 2005 Directed assembly of ZnO nanowires on a Si substrate without a metal catalyst using a patterned ZnO seed layer *Nanotechnology* **16** 292–6

[15] Chaudhry V, Ramamurthi F and Islam M 2007 Ultra-low contact resistance of epitaxially interfaced bridged Si nanowires *Nano Lett.* **7** 1536–41

[16] Conley J F, Stecker L and Ono Y 2006 Selective growth and directed integration of ZnO nanobridge devices on Si substrates without a metal catalyst using a ZnO seed layer *J. Electron. Mater.* **35** 795–802

[17] Gao P X, Liu J, Buchine B A, Weintraub B, Wang Z L and Lee J L 2007 Bridged ZnO nanowires across trenched electrodes *Appl. Phys. Lett.* **91** 142108

[18] Cheng C, Lei M, Feng L, Wong T L, Ho K M, Fung K K, Loy M M T, Yu D P and Wang N 2009 High-quality ZnO nanowire arrays directly fabricated from photoresists *ACS Nano* **3** 53–8

[19] Li P G, Tang W H and Wang X 2009 Synthesis of ZnO nanowire arrays and their photoluminescence property *J. Alloys Compounds* **479** 634–7

[20] Li P G, Wang X and Tang W H 2009 Facile route to well-aligned ZnO nanowire arrays *Mater. Lett.* **63** 718–20

[21] Ranganathan S, McCreery R, Majji S M and Madou M 2000 Photoresist-derived carbon for microelectromechanical systems and electrochemical applications *J. Electrochem. Soc.* **147** 277–82

[22] Du R B, Ssenyange S, Aktary M and McDermott M T 2009 Fabrication and characterization of graphitic carbon nanostructures with controllable size, shape, and position *Small* **5** 1162–8

[23] Park B Y, Taherabadi L, Wang C L, Zoval J and Madou M J 2005 Electrical properties and shrinkage of carbonized photoresist films and the implications for carbon microelectromechanical systems devices in conductive media *J. Electrochem. Soc.* **152** J136–43

[24] Zhai T Y, Fang X S, Liao M Y, Xu X J, Zeng H B, Yoshio B and Golberg D 2009 A comprehensive review of one-dimensional metal-oxide nanostructure photodetectors *Sensors* **9** 6504–29

[25] Lepselter M P and Sze S M 1968 An insulated gate field effect transistor using Schottky barrier contacts for source and drain *Proc. IEEE* **56** 1400

[26] Urnar A, Park Y K and Hahn Y B 2009 High aspect-ratio ZnO nanowires based nanoscale field effect transistors *J. Nanosci. Nanotechnol.* **9** 2692–97

[27] Li Q H, Gao T, Wang Y G and Wang T H 2005 Adsorption and desorption of oxygen probed from ZnO nanowire films by photocurrent measurements *Appl. Phys. Lett.* **86** 123117

[28] Li Y B, Della Valle F, Simonnet M, Yamada I and Delaunay J J 2009 Competitive surface effects of oxygen and water on UV photoresponse of ZnO nanowires *Appl. Phys. Lett.* **94** 023110

[29] Feng X J, Feng L, Jin M H, Zhai J, Jiang L and Zhu D B 2004 Reversible super-hydrophobicity to super-hydrophilicity transition of aligned ZnO nanorod films *J. Am. Chem. Soc.* **126** 62–3

[30] Goldberger J, Sirbuly D J, Law M and Yang P 2005 ZnO nanowire transistors *J. Phys. Chem.* B **109** 9–14

[31] Huang M H, Wu Y Y, Feick H, Tran N, Weber E and Yang P D 2001 Catalytic growth of zinc oxide nanowires by vapor transport *Adv. Mater.* **13** 113–6

[32] Wan Q, Li Q H, Chen Y J, Wang T H, He X L, Li J P and Lin C L 2004 Fabrication and ethanol sensing characteristics of ZnO nanowire gas sensors *Appl. Phys. Lett.* **84** 3654–6